Journal of Hydrology 643 (2024) 132021

Contents lists available at ScienceDirect

Journal of Hydrology

journal homepage: www.elsevier.com/locate/jhydrol

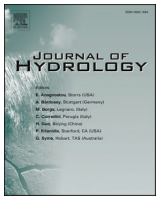

Research papers

High spatiotemporal resolution free surface detection using cost-effective video equipment and computer vision techniques in nearly stationary flow along a transparent wall in the laboratory

Ricardo Martins [a,*], Jorge M.G.P. Isidoro [b,c], João L.M.P. de Lima [d,e]

[a] RISCO - Research Center for Risks and Sustainability in Construction, Department of Civil Engineering, University of Aveiro, 3810-193 Aveiro, Portugal
[b] Department of Civil Engineering, Institute of Engineering, University of Algarve, Campus da Penha, 8005-139 Faro, Portugal
[c] CIMA – Centre for Marine and Environmental Research / ARNET - Aquatic Research Network, University of Algarve, Campus de Gambelas, 8005-139 Faro, Portugal
[d] MARE - Marine and Environmental Sciences Centre / ARNET-– Aquatic Research NETwork, Rua da Matemática, 49, 3004-517 Coimbra, Portugal
[e] Department of Civil Engineering, Faculty of Sciences and Technology, University of Coimbra, Rua Luís Reis Santos, Pólo II – University of Coimbra, 3030-788 Coimbra, Portugal

ARTICLE INFO

This manuscript was handled by Sally Elizabeth Thompson, Editor-in-Chief, with the assistance of John Quilty, Associate Editor

Keywords:
Hydrometry
Free surface detection
Computer vision
MATLAB®

ABSTRACT

The identification of the air–water interface in free surface flows traditionally involves intrusive techniques or costly equipment. Non-intrusive alternatives, such as computer vision, are emerging as highly effective substitutes or supplements for more invasive techniques in laboratory measurements, thanks to their straightforward implementation and cost efficiency. This research specifically delves in the conjunction of various naive techniques, exploring their collective precision in detecting the air–water interface along transparent walls in laboratory. A detection technique based on the double gradient of the image is applied and thoroughly examined. The study progresses through multiple refinement stages, culminating in a method that is both cost effective and easy to implement. This methodology allows for large-scale, high resolution measurements (200 mm × 1800 frames per video at a 0.25 mm, 50 Hz resolution), offering both spatial and temporal measurements by adeptly detecting the free surface along transparent walls.

1. Introduction

Computer vision is based on the automatic acquisition of images from video equipment and their interpretation using specific algorithms aimed at extracting visual information. Computer vision based techniques aim to automate tasks usually performed by the human visual system (Forsyth and Ponce, 2002). These techniques have been used in the most diverse fields. Nonetheless, one of the most common uses of computer vision is the measurement of distances and dimensions, e.g., (Jawad and Husain, 2017; Leo et al., 2017). In hydraulics and hydrology, the measurement of water depths or the monitorisation of the surface water level are essential for a wide range of applications, both in the realm of research and within industry, such as river hydrometry (Zhang and Tong, 2023), water supply systems, water and wastewater treatment plants (Nguyen et al., 2009), irrigation channels, laboratory physical models (Gilmore et al., 2013), water resources optimisation, measuring surface velocity (Huang et al., 2022), among others. The most common techniques to measure the water depth or water level include direct (human eye) observation of the water surface against a scale, automated sensors (ultrasonic, infrared, and laser) and pressure probes. In the laboratory, the point-gauge micrometre is still widely used, namely for research and educational purposes. Further traditional techniques for water level and water depth measurements are explored and described in Herschy (2008), Bertrand-Krajewski et al. (2008), or Loizou and Koutroulis (2016).

The accurate measurement of water depths using sensors and probes is subject to certain limitations, often arising from localised perturbations, such as those caused by resistive probes. These disturbances inevitably introduce biases into the readings and measurements, thereby affecting the precision of the data collected. Non-intrusive methods such as ultrasonic, infrared, and laser methods, are acknowledged for their limitations – cost, and they often measure only small sections or points. Sensors and probes cannot measure along space (longitudinally), unless they are mounted in specific support systems, usually with complex

* Corresponding author.
E-mail address: ricardo.d.martins@ua.pt (R. Martins).

https://doi.org/10.1016/j.jhydrol.2024.132021
Received 17 April 2024; Received in revised form 19 August 2024; Accepted 2 September 2024
Available online 16 September 2024

geometries and operation procedures that must be tailor-made, entailing another major limitation. Moreover, the cost of acquisition and maintenance (e.g., regular scheduled calibration) of this sort of equipment cannot be disregarded. The limitations of using sensors and probes to measure water depths can be overcome by using remote sensing techniques. These non-intrusive techniques (*i.e.*, that do not explicitly change the flow pattern or behaviour), based on Radio Detection and Ranging (RADAR), Light Detection and Ranging (LIDAR), ultrasonic or infrared waves, and on digital images or videos, are becoming a widespread alternative for water depth/level measurements (Majdalani et al., 2019).

Digital images and videos, as well as the methods for imagery processing and treatment, are non-intrusive new ways for data processing (e.g., automatic identification, pattern recognition, and machine learning) without disturbing the flow, opposite to, e.g., resistive probes (Isidoro et al., 2021). With the massification and consequent price reduction of digital video cameras, researchers have been working utilising these equipment and methods in fields that, just a few years ago, would have demanded much costlier and specialised equipment. In fact, developments in optical materials and signal processing hardware allowed the design and construction of smaller and feature-packed digital cameras that can take high-resolution pictures (Sinha, 2012). Imagery from these digital cameras have been recently used in several types of hydrometric measurements, such as laboratory open-channels (Isidoro et al., 2021), flood events (Chaudhary et al., 2020), or wastewater drainage (Ji et al., 2020).

Computer vision based techniques have been used most recently for real-time water level measurement and monitoring. This is particularly relevant, as extracting water level information from image and video data are not easy tasks, as it is inherently difficult to segment water (Jafari et al., 2021). These difficulties can also originate from environmental conditions such as camera position instability (e.g., Lin et al., 2018) or different sunlight intensities (e.g., Kuswidiyanto et al., 2021). Lin et al. (2018) tackled the difficulties caused by changes in camera orientation and heavy-weather conditions applying object-based image analysis, image matching, and photogrammetric techniques to images acquired by a single camera. This automatic measuring system, designed to be used in man-made facilities (e.g., channels and reservoirs), allowed to obtain measurements with a resolution up to 10 mm, but only with relatively still water levels. The use of computer vision based techniques for measurement of water levels has been used with success in several types of hydraulic facilities. Kuswidiyanto et al. (2021) developed a water level monitoring system for irrigation management. The system automatically captures irrigation channel staff gauges (metal ruler near a Parshall flume) and identifies the water level with a precision of 0.01 m, where the water level can range from 0 to 1 m. However, the automatic measurement system suffered from errors caused by changes in sunlight conditions and inconsistencies on image capture angle, distance, and elevation. Sabbatini et al. (2021) also presented an automatic measuring system for staff gauges, but for river flood monitoring. In their work, the authors addressed issues related to the lack of natural light, *i.e.*, the possibility of using the system in daytime and lowlight conditions (even in nighttime), and to reliability during bad weather (being able to operate during extreme weather conditions). This system was designed to detect the water level with a precision of approximately 30 mm. Another example of an automated river flood detection system was presented by Fernandes Jr. et al. (2022) who used deep neural networks for segmentation of the water surface and computer vision to estimate the water level. This system included a calibration step where a reference line had to be manually drawn; however, eliminating the need for novel parametrisation. This automated detection system showed to be successful in dealing with different camera viewpoints and lighting conditions, attaining an accuracy of 33.2 mm in the tests carried out by the authors. Noto et al. (2022) used a low-cost near-infrared wildlife camera to monitor the water level with a resolution of about 20 mm in intermittent and ephemeral streams. The use of a near-infrared camera pointing at a white-painted steel pole, helped to mitigate the hinder that low-light conditions, such as nighttime, pose to computer vision techniques to measure water levels/depths. Nonetheless, due to the camera battery and data storage capacity, images were acquired with a 30-minute interval. Imagery obtained from social media have been also used recently to measure water levels. Jafari et al. (2021) developed a deep learning based segmentation algorithm able to process large amounts of data from images and videos acquired from social media and permanent infrastructure, e.g., road traffic cameras, for urban flood management. The authors used advanced object-based image analysis techniques for faster, although accurate, water segmentation, where objects detected in images and videos provided references to estimate water levels along time. These examples give evidence that using computer vision techniques to measure and monitor water level/depth is not a straightforward task. Moreover, the improvement of the imagery quality and the optimisation of its acquisition environment are not the only challenges for the application of these techniques, and a continuous improvement of the image processing algorithms is also essential for the successful use of computer vision techniques in hydrometry (Lan et al., 2020)

While other algorithms showed to be already partially effective (e.g., Isidoro et al., 2021), some naive approaches were required to achieve a stable solution. Spurious values, which occurred mainly when reflections of the bottom were almost horizontal, or the bottom was straight, led to erroneous line detection, which could be either removed or corrected using temporal and spatial moving averages. This introduced uncertainties often above one pixel, hampering the intended high-resolution and introducing uncertainty into the process. The objective of this novel methodology is to either reduce or eliminate these sorts of discrepancies.

The measurement and monitoring of water depths and levels is fundamental for various applications. The use of computer vision based techniques for these purposes is thus gaining significant attention due to the non-intrusive, cost-effective, and continuous measurement capabilities, both in space and time. This study aims to develop and propose a technique that can measure fluctuations in the free surface of channels with transparent walls such as glass, acrylic, or crystalline plastic, typically used in laboratory channels. Specifically, this work provides: (1) an insight on the conjunction of several techniques and their effectiveness when grouped for the detection of the air–water interface; (2) a novel technique based on the double gradient of the image; (3) parameters optimised for the test case presented; (4) a cost effective and easy implementation methodology. The proposed methodology uses image treatment and segmentation techniques to automatically detect the free surface in open-channels. Two key-improvement over existing techniques are achieved by subtracting the background from the images and by applying a double gradient in the edge detection, leading to a more accurate detection and segmentation of the flow's free surface. The high-resolution (to the pixel size) and real-time measurements (applied to single frames) acquired through this method can provide valuable insights for a wide range of applications. To evaluate the effectiveness of the proposed technique, experiments were conducted using both coloured and colourless water. The results suggest that tinting the water can improve the accuracy of the computer vision based measurements. To validate the results, comparisons were made against measurements obtained using ultrasonic sensors, that are focused on a limited area in the flow. In summary, the present work proposes a novel methodology to improve the quality of depth and level measurements and monitoring in open-channels with transparent walls when using computer vision based techniques.

2. Methodology

The objective of this study was to measure the instantaneous fluctuations of the air–water interface, by detecting the interface per frame, without considering any of the previous frames in the image treatment. As such, the core parameter detected during measurements was the

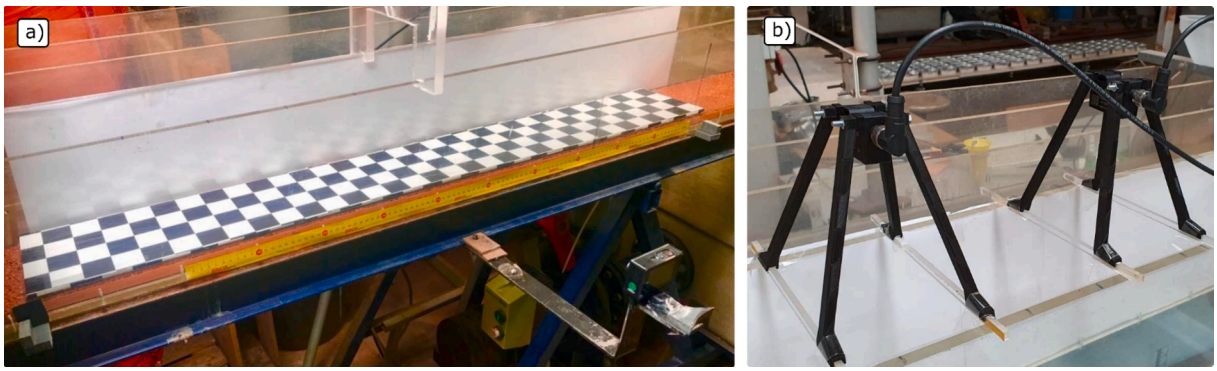

Fig. 1. a) Detailed view of the channel structure, employing a black and white checkerboard solely for geometry control. b) Close-up of the ultrasonic sensors; for this study, data from a single sensor was utilised.

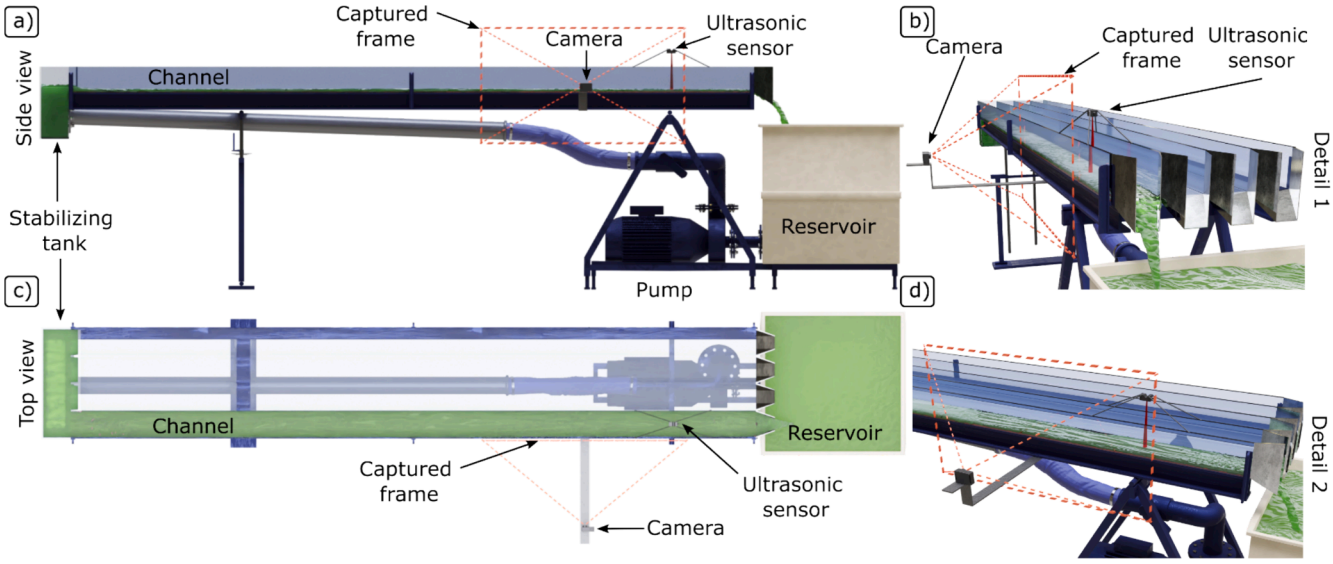

Fig. 2. Schematic depiction of the experimental laboratory flume, with water tinted green to enhance contrast and facilitate visualisation: a) side view; b) detail from downstream; c) top view; d) detail of camera and ultrasonic sensor. (For interpretation of the references to colour in this figure legend, the reader is referred to the web version of this article.)

position of the air–water interface against the acrylic wall of the channel. Having the exact position of the interface, and knowing the bed-water interface, the depth of water is measured by subtracting both values and converting them to real world scale. This study encompasses a four stage development plan with, with various enhancements considered at each stage.

2.1. Experimental apparatus

The flume utilised in this study is housed at the Laboratory of Hydraulics, Water Resources, and Environment which is part of the Civil Engineering Department of the University of Coimbra (Fig. 1).

This flume, featuring four parallel channels as depicted in Fig. 2 has been routinely employed for the systematic investigation of surface hydraulic, hydrological, and ecological processes. The configuration of the flume was customised to optimise its suitability for the specific experimental test conducted.

The closed-circuit system supplying the flume consists of a primary fiberglass reservoir with a capacity of up to 0.5 m^3, connected to a constant velocity centrifugal pump. Flow control in the supply pipe is managed by a ball valve, ensuring precise regulation. The constant head tank, located upstream of the flume and equipped with a turbulence diffuser, is instrumental in maintaining a consistent water level. To ensure controlled flow conditions, the measurement area was positioned 2.5 m from the constant head tank, approximately 15 times the width of the channel. The channel floor incorporates four types of variable rough beds (Isidoro et al., 2023). For data collection, a single high-resolution camera, a GoPro 7 Black, was strategically positioned to capture the vertical plane. It recorded at 1920 × 1080 pixels and 50 frames per second. A white background (white paper) placed behind the furthest channel wall enhanced contrast in the interface, minimising background reflections on the acrylic walls. The flume ends with a free-fall outlet designed to induce supercritical flow conditions, without affecting upstream flow dynamics.

During the development and validation phases of this study, a series of tests were made using an experimental multipurpose flume. Despite the flume has four parallel acrylic channels, each measuring 4.00 m in length, 0.15 m in width, and 0.20 m in height (L × W × H), only one channel was used for this investigation, with different bed to simulate several hydraulic roughness. Video acquisition and recording processes were monitored throughout the entire experimental duration. The detection of the free surface, using four bed roughness levels to induce a higher or smaller longitudinal free surface variation, was evaluated along with tinted and untinted water, and three water discharges leading to different reference depths. Tinted water was obtained by adding a green food colourant to the water, for additional contrast and to

Table 1
Main experimental flow, fluid, and channel parameters.

Bed roughness (d_{50}) [mm]	Water reference depth [mm]	Water colour
0 (R0)	5 (F5)	Tinted
1.5 (R1)	10 (F10)	Untinted
3.4 (R2)	15 (F15)	
6.4 (R3)		

replicate high turbidity conditions that might be found in the field. The flume slope was positioned at 1 % in all the experimental runs. To video-record the tests, a GoPro Hero 7 camera was positioned perpendicularly to the flume's acrylic wall and set to record at a resolution of 1920 × 1080 and 50 fps. The camera's software corrected the eventual lens distortion using linear mode. Each experimental run was recorded for at least 60 s with the data analysed for the middle interval of 30 s, resulting in 1500 frames per bed roughness and per water reference depth, summing up to a total of 18,000 frames for which the air–water interface was obtained. Prior to all tests, the water was allowed to flow in the channel for approximately three minutes to ensure a steady state. Table 1 provides an overview of the primary conditions under which the laboratory tests were conducted, where water reference depth regards the approximate depth set up prior to each experimental run. R# regards the bed roughness (d_{50}) and F# regards the approximate initial depth of water (reference depth).

The tests carried out during this study followed four steps (stages), with progressive enhancement of the developed computer vision technique. The first set of tests (first step – Stage 1) involved the use of a computer vision based method under artificial lighting. In the second stage, the technique was enhanced through the incorporation of an algorithm specifically designed to virtually eliminate the flume background and channel bed, aiming to improve the water surface detection and segmentation, thus leading to higher accuracy in water level and depth measurements. Artificial lighting was used during this second step (Stage 2). During the third step of testing (Stage 3), the virtual removal algorithm was utilised under natural lighting conditions, with water tinted with green food colorant. Finally, during the fourth and last testing step (Stage 4), the background and channel bed virtual removal algorithm was applied with tinted water under natural lighting conditions. In this final step, ultrasonic distance measuring sensors (Baumer, model U500.DA0.AA1B.72O) were also used to measure water depth, allowing for benchmarking against the proposed computer vision based technique. This type of ultrasonic sensor has a scanning range of 100–1000 mm with a resolution under 0.3 mm. A detailed discussion of these testing steps can be found in the following sections.

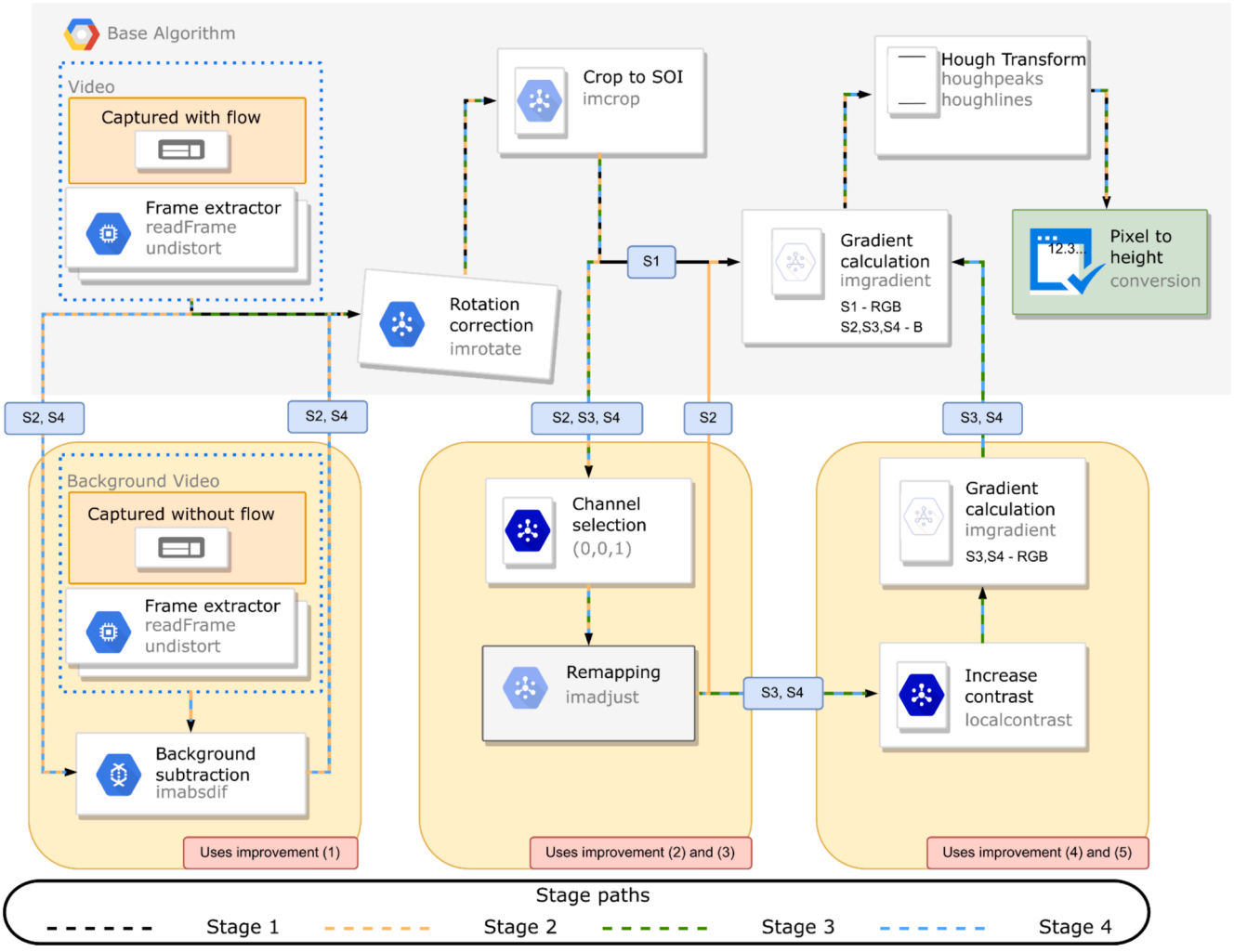

Fig. 3. Flowchart illustrating the stages of the FRACTAL algorithm: frame extraction, Section-Of-Interest (SOI) definition, image gradient calculation using Sobel and Feldman methodology, and application of the Hough Transform algorithm to identify the free surface. Each coloured path corresponds to a stage in the flowchart (Stage 1, 2, 3, and 4), with associated improvements indicated by (#) in red. (For interpretation of the references to colour in this figure legend, the reader is referred to the web version of this article.)

Table 2
Sequence of the different experimental stages and improvements.

Stage	Artificial lighting	(1) Background subtraction	(2) Channel selection	(3) Remapping	(4) Increasing contrast	(5) Gradient weighting	Water colouring
1	Yes	No	No	No	No	No	No
2	Yes	Yes	Yes	Yes	No	No	No
3	No	No	Yes	Yes	Yes	Yes	Yes
4	No	Yes	Yes	Yes	Yes	Yes	Yes

2.2. Algorithm

2.2.1. Enhanced FRACTAL algorithm

The initial step of FRACTAL (Free suRfACe deTection Algorithm) involves extracting frames from a video (Fig. 3).

Each of these frames undergoes variable digital exposure (*i.e.*, the time the camera captures the image in the sensor) and aperture settings (*i.e.*, the amount of light that the sensor reads). Due to this automatised process, some images might have a large digital exposure and low aperture which can lead to blurring caused by fast motion (*i.e.*, the amount of time the sensor records the image can lead to the interface being captured in different pixels in the sensor and hence create blur in the frames). This is a process that is common to cameras and sensor alike since complete instantaneous measurement often requires expensive equipment. While the vertical variation of the free surface is typically not instantaneous and can be accurately measured using 10 Hz instrumentation, the first stage of the FRACTAL algorithm uses a higher frequency of 50 Hz (fps) to minimise the amount of motion blur in the frames, thus obtaining a more accurate and pronounced edge.

In the second stage of FRACTAL, a correction is applied to remove lens distortion and adjust for small movements of the camera. Failure to apply this correction can affect accuracy, causing pixel values to appear curved instead of flat. FRACTAL utilises the de-distorting algorithm provided by the GoPro hardware. In this study, the Section-of-interest was limited to a horizontal centre band, avoiding corners where lens distortion could influence results. The camera remained fixed and parallel to the channel throughout the study, so image stabilisation was not used. However, if the camera is disturbed during measurement, image stabilisation can be applied cautiously, as it may alter pixel values and compromise accuracy.

The third step of FRACTAL regards the definition of a Section-Of-Interest (SOI) to be measured and crop the image accordingly. A full frame analysis is not always necessary, and a Region-Of-Interest (ROI) is used to act as a "window" that sweeps throughout the SOI, in the frames to be measured. The SOI, spanning 700 pixels in length and 195 pixels in height, was defined to encompass all areas pertinent for analysis, effectively excluding non-relevant background areas. This optimisation, translating to 193 mm by 50 mm, was implemented to ensure computational efficiency while maintaining the relevance of the analysed section. By focusing computational resources on the essential areas of interest, this approach streamlined the analysis process and enhanced the accuracy of the study's findings. Seven values are provided, divided into two categories: (a) the width and height of the SOI along the y and x coordinates of the bottom-left corner, and (b) the width, height, and advance of the ROI (*i.e.*, the number of pixels the ROI advances with each measurement, which was set to 1 in this study).

The fourth step of FRACTAL involves calculating the gradient of the image using the Sobel and Feldman (1968) methodology, which considers a weighted sum of pixels in a 3 × 3 neighbourhood, thus highlighting the highest differences in luminosity from pixel to pixel. This procedure plays a central role in detecting the free surface, as it clearly distinguishes the air–water interface. The *Sobel and Feldman* method is then applied to calculate the edges by identifying the areas where the absolute differences in luminosity are the highest, which mathematically correspond to the second derivative of the original image with respect to its luminosity.

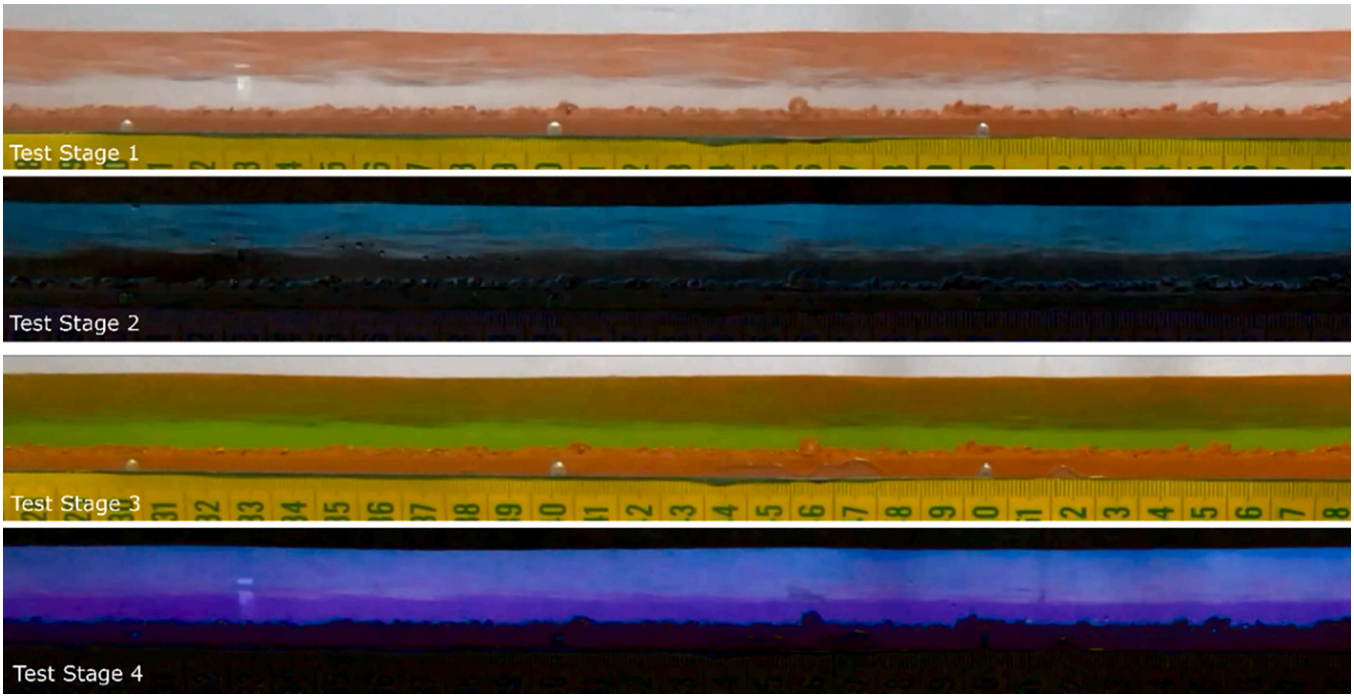

Fig. 4. Results of the background subtraction technique applied to the free surface depth measurement algorithm. Stages 1 and 3 show images without background subtraction, while Stages 2 and 4 illustrate the effects of background subtraction.

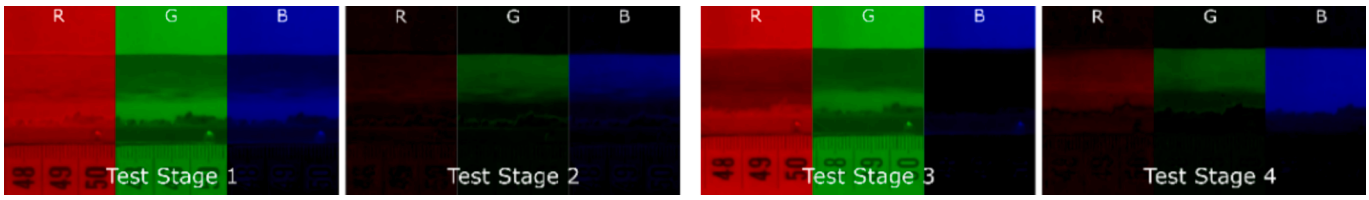

Fig. 5. RGB channels for the four stages of the enhanced FRACTAL algorithm highlighting the importance of blue channel. (For interpretation of the references to colour in this figure legend, the reader is referred to the web version of this article.)

Finally, the output image is processed by the Hough Transform algorithm, which identifies the longest straight line in the ROI, considering it as the representation of the free surface.

2.2.2. Improvements

Several improvements, detailed in See Table 2, were implemented to enhance accuracy and minimise spurious values.

(1) Background subtraction – The FRACTAL algorithm employs a background image of the SOI captured prior to the experiments. This background image is subtracted from each frame of the video, channel by channel (RGB), and pixel by pixel, (using in MATLAB's *imabsdiff)*. The background subtraction technique effectively enhances the air–water interface, which is the only changing (dynamic) component in the image. Fig. 4 depicts the results of the testing process, where Stages 1 and 3 show images without background subtraction, while Stages 2 and 4 illustrate the effects of background subtraction.

(2) Channel selection – The blue channel is selected as the representative channel while the other channels (red and green) are disregarded for all subsequent operations. This selection is crucial for two reasons. Firstly, the background subtraction process results in a predominantly blue image, as illustrated in Fig. 2, Stages 2 and 4. Secondly, in the Stage 1 and 3 images, the blue channel provides the highest contrast at the air–water interface. This is caused by the absence of blue in the water and the abundance of blue in the white wall behind, further highlighting the importance of the blue channel selection. Examples of the image partitioned into RGB and untinted water are illustrated in Fig. 3 for the four stages of the enhanced FRACTAL algorithm.

Choosing the blue channel to analyse the images provides a distinct advantage as seen in Fig. 5, Stage 4 (B). When the water is tinted, the background removal process results in higher contrast edges for the interfaces between the water, air, and the bed, appearing almost black against the surrounding areas. This contrast is not visible with the other colour channels, which either only highlight reflections under the water's free surface or produce a smeared edge that is challenging for the algorithm to detect.

(3) Remapping – The redefinition of the subtracted image is enhanced by remapping the blue channel's intensity values. A low-pass filter with a value of 0.1 and a high-pass filter with a value of 0.7 are applied to the blue channel. This effectively filters out low blue intensities (near-black areas) and high blue intensities (near-white areas) respectively, resulting in a more accurate representation of the air–water interface. To ensure consistency across experiments, the filtered blue channel was normalised to the full range of 0 to 1. It is important to note that the filter values should be configurable and adjusted for each experiment, as they may vary with different lighting conditions and background colours.

(4) Increasing contrast – The contrast of the cropped ROI is further enhanced by applying a local contrast enhancement (using in MATLAB's *localcontrast),* for each ROI. This augments the local contrast by smoothing low gradient areas while retaining strong edges, as illustrated in Fig. 5 by the difference between Stages 1 and 3, and Stages 2 and 4. However, to obtain optimal results, the values for the *localcontrast* function parameters *edgeThreshold* and *amount* require calibration. In the experiments carried out during this investigation, values of 0.4 and 0.5, respectively, were found to be optimal. Nonetheless, these values may need to be adjusted when conducting experiments under different conditions (e.g., luminosity, colour/turbidity of water).

(5) Gradient weighting – An additional step has been added to the edge calculation process, where the images are weighted by considering not only the edge of the blue channel's gradient ($\nabla(\nabla \boldsymbol{B}(i,j))$), but also the gradient of the blue channel itself ($\nabla \boldsymbol{B}(i,j)$). The resulting matrices from the edge detection process undergo a weighted sum, where a weight of 2 is applied to the edge computed from the gradient, and a weight of 1 is applied to the edge calculated from the blue channel. This weighting scheme allows for a more balanced consideration of the information provided by the two sources, resulting in a final output image ($\boldsymbol{E}(i,j)$). The $\boldsymbol{E}(i,j)$ pixel value can go up to 3. As such, to ensure that both the maximum values of $\nabla \boldsymbol{B}(i,j)$ and $\nabla(\nabla \boldsymbol{B}(i,j))$ are captured in the final matrix, a filtering threshold to limit the maximum values to 1 was applied obtaining this way the final matrix $\boldsymbol{E}(i,j)_H$.

$$2\nabla(\nabla \boldsymbol{B}(i,j)) + \nabla \boldsymbol{B}(i,j) = \boldsymbol{E}(i,j)$$

$$\boldsymbol{E}(i,j)_H = \begin{cases} 1 & if \quad \boldsymbol{E}(i,j) > 1 \\ 0 & if \quad otherwise \end{cases}$$

Because image conditions such as brightness/luminosity, contrast, and camera quality may vary, adjustments to specific parameters are needed for improvements (3) and (4). Table 2 provides a summary of the followed sequence of test stages and improvements made during the experimental procedures.

2.2.3. Water tinting

The interface detection process relies on evaluating the colour, gradient, and luminosity of the matrices. To improve this process accuracy, it is decisive that the bed and water have distinct colours from the background. Ideally, the bed and water should also have different colours from each other to better enable the bed detection. It was observed that in the case of crystal clear water, reflections beneath the free surface result in false detections, due to the presence of several steep gradients in the same image. To enhance the contrast between the bed, water, and air, distinctive colours for each of these were enforced. These distinctive colours serve as a differentiation factor, making it appropriate to tint the water to simulate turbidity conditions. Green was chosen as the colour for the water since the beds were predominantly red and the background was white. To achieve this, a biodegradable food additive, composed of "Green S" (Moozyckine and Davies, 2002) and "Quinoline Yellow" (Gupta et al., 2005), was dissolved at a concentration of 1.25×10^{-4} l/l and thoroughly mixed in water, resulting in the configuration depicted in Fig. 5, Stage 3.

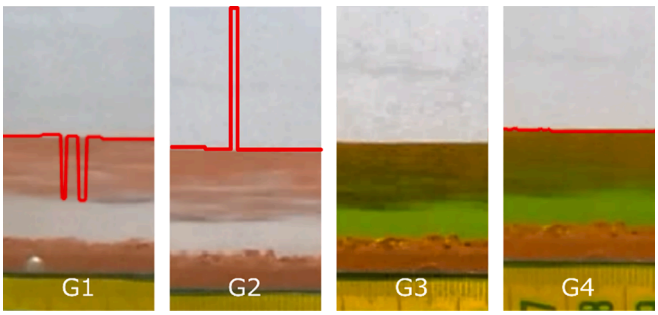

Fig. 6. Examples of measurements categorised within the different groups: G1 – below the free surface; G2 – above the free surface; G3 – non-detections; G4 – accurate detections.

3. Results and discussion

FRACTAL was applied to each frame extracted from the videos, independently from the other frames, across all the bed roughness and water reference depths. This yielded 1500 frames per roughness and flow condition, summing up to a total of 18,000 frames where the air–water interface was detected. The Section-Of-Interest was defined as a window of the total captured frame.

Pixel size was calculated by using several sections predefined in the image, each with 10 mm length, and 39 pixels in the horizontal and vertical direction, resulting in a square pixel with real world dimension of 0.256 mm × 0.256 mm.

Groups and results, obtained during each of the four stages, are exemplified in Fig. 6 and presented in Figs. 7–10 respectively. To complement the analysis Figs. 13–16 are presented in Appendix A. Each figure corresponds to a distinct stage of the tests and comprises the 12 tests conducted within that stage. The 3D plots depict the depth detected on the vertical axis, the column in pixels on the x-axis, and the time or frame on the y-axis. These images provide a comprehensive evaluation of the surface dynamics over time and space. For a holistic understanding, it is recommended to refer to Figs. 7–10 concurrently with Figs. 13–16. In the first stage, the FRACTAL algorithm was used with artificial lighting conditions and without any other enhancements (see Table 2). In the second stage, background subtraction was added along with enhancements (2) and (3). In the third stage, the artificial lighting was removed, the water was tinted, and enhancements (4) and (5) were added while background subtraction (1) was removed. In the fourth stage, background subtraction was added once again, and the data was compared against data acquired from an ultrasonic sensor. The comprehensive analysis of each experimental step enables a thorough understanding of the advancements made, particularly in the accuracy of depth/level measurement through the implementation of the techniques here described.

For each individual stage, each section in Figs. 7–10 represents a combination of different beds (R0–R3) with the subsequent reference depth (F5–F15). Statistical functions, namely minimum, first quartile, average, third quartile, and maximum were plotted against the left vertical axis in a symmetrical 10 base logarithmic scale (negative differences are plotted as negative values, as the logarithm function cannot be negative). The standard deviation and pixel size used for this study were presented against the right vertical axis in a logarithmic scale. The left axis represents the deviation from the mode, for each pixel along the spatial resolution. The mode was taken as the reference value. This assumption is reasonable regarding hydraulics since the oscillations that occur during steady state are often small and the most frequent value is often the most correct. Mode neglects the effect of very large outliers, whilst average does not. As such, if extreme values are detected, far from the correct value, their effect in the analysis is unaccounted, something that would not happen with the average should it be used as the reference value. Unsteady tests were not conducted as Isidoro et al. (2021) proved that for, the temporal sampling (50 Hz) used in this study, if the algorithm is able to capture steady state variations, without using the previous time step, then the methodology will also detect unsteady variations.

The results were categorised into four groups (*G#*) each delineating the dominant characteristic of the detection observed in the measured values, as detailed in Table 3.

In the first group of tests (*G1*) spurious measurements are mostly due to reflections detected in the underside of the free surface, mostly in the farthest section of the channel. The second group (*G2*) included tests

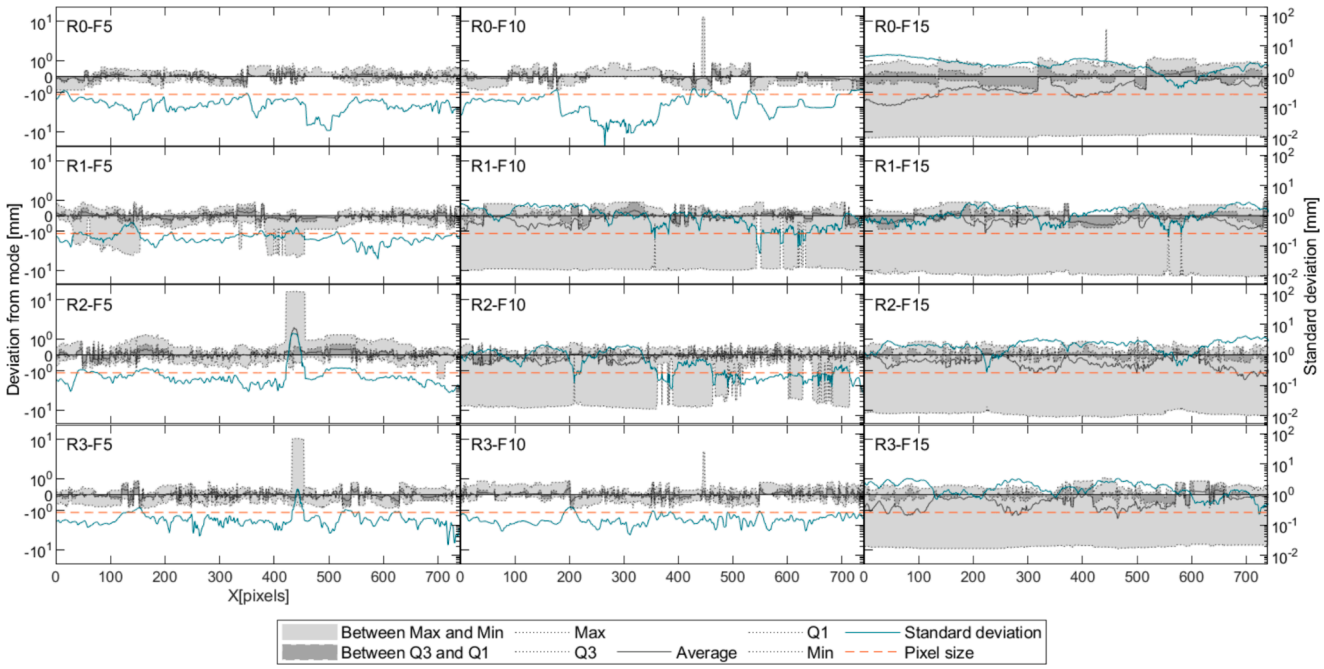

Fig. 7. Temporal statistics of pixel measurements along the SOI using the FRACTAL algorithm (Stage 1). The graphs depict the detection rates and variations for different flow rates. The left vertical axis relates to greyscale values while the right axis relates to colour values.

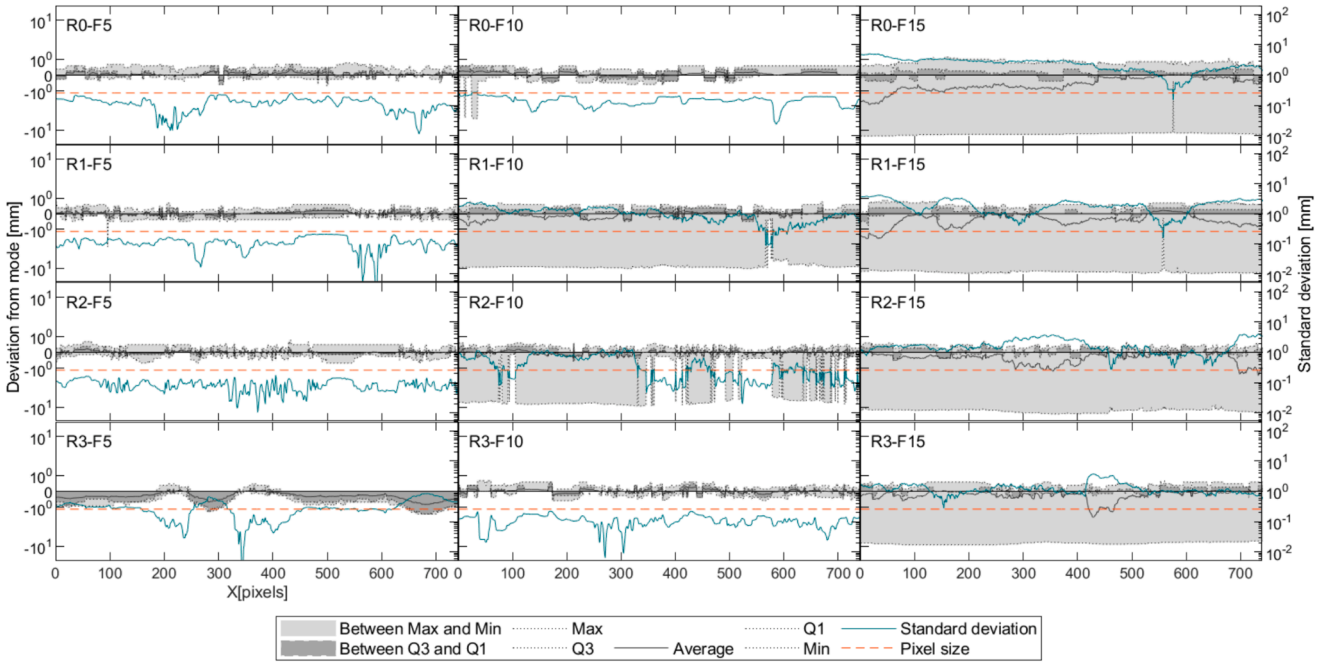

Fig. 8. Temporal statistics of pixel measurements along the SOI using the FRACTAL algorithm (Stage 2). The graphs depict the detection rates and variations for different flow rates. The left vertical axis relates to greyscale values while the right axis relates to colour values.

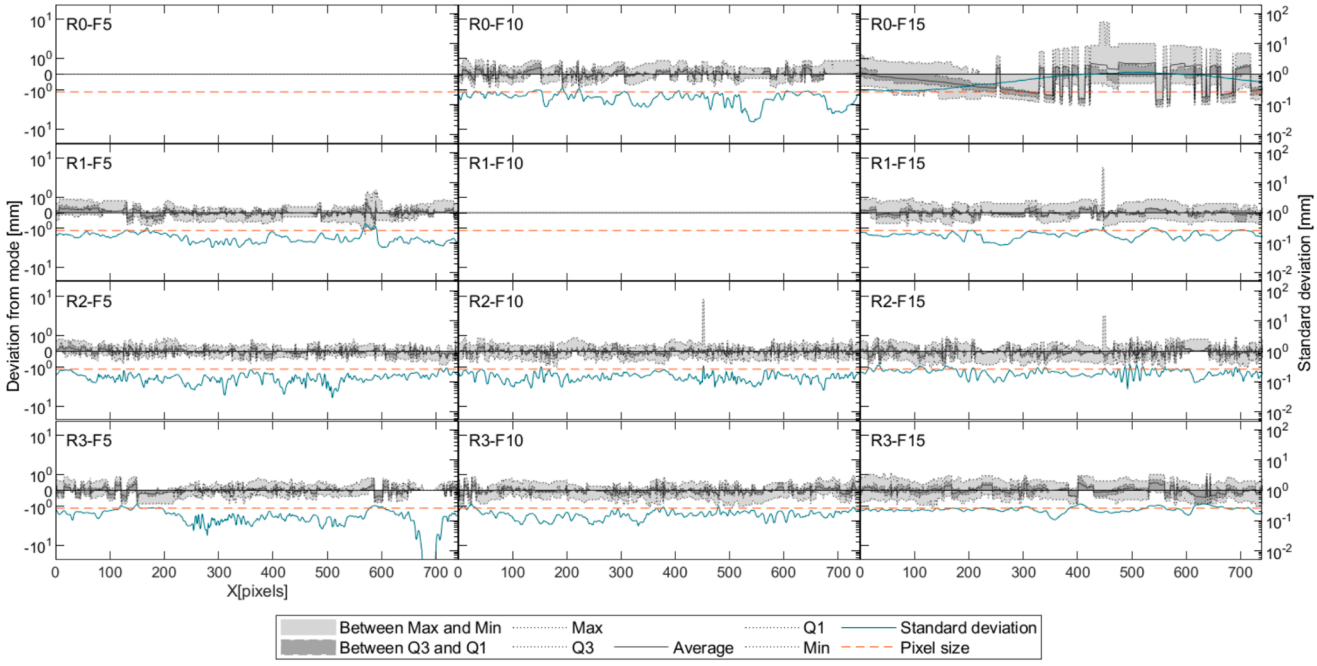

Fig. 9. Temporal statistics of pixel measurements along the SOI using the FRACTAL algorithm (Stage 3). The graphs depict the detection rates and variations for different flow rates. The left vertical axis relates to greyscale values while the right axis relates to colour values.

where some detections occurred above the interface, *i.e.*, completely in the air section, including the highest point of the SOI/ROI. The third group (*G3*) comprised tests with non-detections, *i.e.*, where the surface was not detected (continuously or partially), irrespectively of whether there was any output from the algorithm or not. The fourth group (*G4*) consisted of detections that seemed accurate and exhibited minimal variation, with at least 99 % of the points being accurately detected. Fig. 6 shows examples of the free surface detection for the four groups considered.

3.1. Algorithm improvements analysis

The four-stage process outlines a systematic approach to improving the accuracy and reliability of measurements of the several improvements of the FRACTAL algorithm. This process progressively tackles specific challenges encountered in detecting surface flow dynamics. Each stage builds upon insights from the previous one, leading to a comprehensive assessment of the algorithm's performance across varied laboratory experimental conditions. Stage 1 focused on evaluating the algorithm's performance under artificial lighting conditions. Stage 2

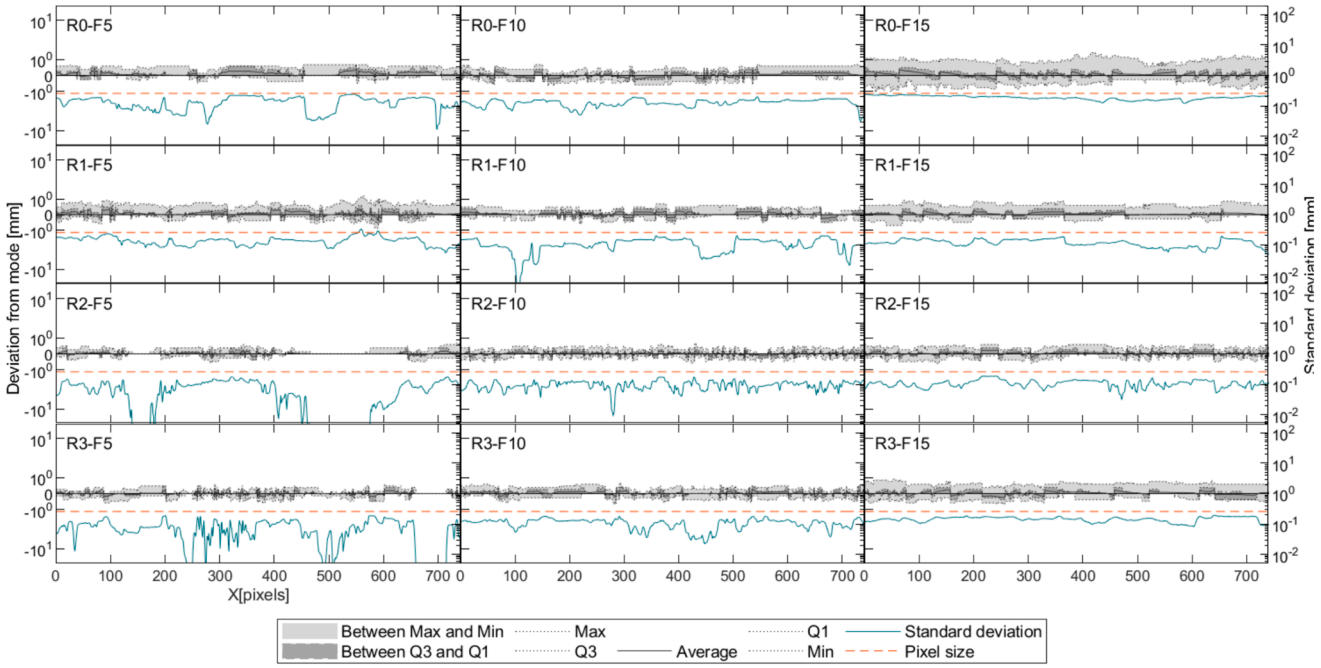

Fig. 10. Temporal statistics of pixel measurements along the SOI using the FRACTAL algorithm (Stage 4). The graphs depict the detection rates and variations for different flow rates. The left vertical axis relates to greyscale values while the right axis relates to colour values.

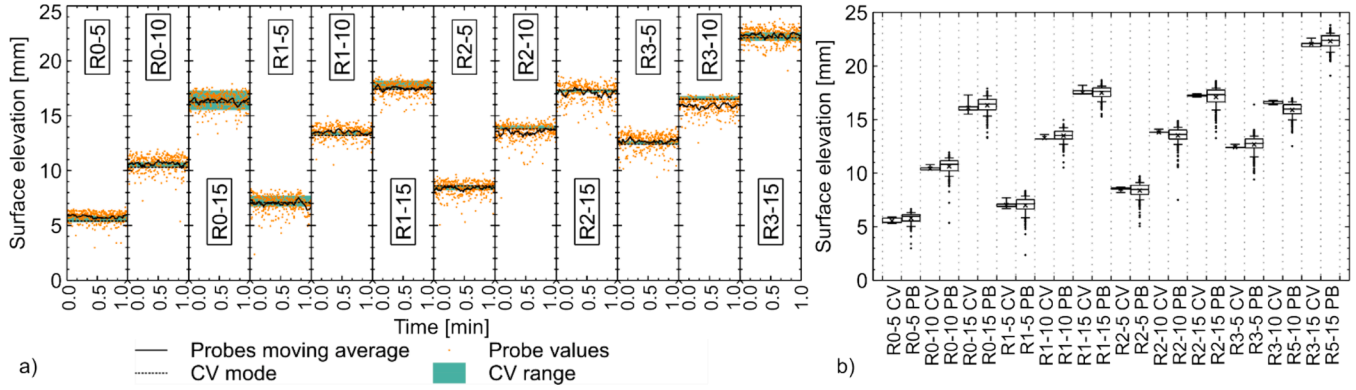

Fig. 11. a) Comparison of surface elevation measurements using fractal computer vision technique (CV) as the mode (black dotted line) and range (green area), alongside the ultrasonic probe (PB) as points (orange points) and moving average (black line) for each test; b) Boxplot of the ultrasonic probe (PB) results and the FRACTAL computer vision technique (CV) for each test. (For interpretation of the references to colour in this figure legend, the reader is referred to the web version of this article.)

then incorporated enhancements such as background subtraction and channel selection based on insights from Stage 1. Stage 3 involved assessing the algorithm using tinted water to simulate natural turbidity or the presence of coloured particles, without background subtraction and artificial lighting. Finally, Stage 4 introduced additional experimental conditions for testing the FRACTAL algorithm. This included background subtraction, channel selection, increased contrast, gradient weighting, and tinted water, further expanding the scope of evaluation. These stages are presented to systematically address various challenges encountered in the detection of surface flow dynamics in laboratory and to provide a thorough evaluation of the FRACTAL algorithm's improvements performance across a range of realistic experimental conditions in laboratory, ensuring its robustness and applicability in a wider range of scenarios.

Each stage's results will be presented as a figure consisting of twelve sub-figures showing temporal statistics for the analysed Section-Of-Interest (SOI). The horizontal axis represents the longitudinal length of the SOI, while the left vertical axis shows the deviation from the mode, and the right vertical axis displays the standard deviation and pixel size. Statistical values such as Max, Q3, Average, Q1, and Min are depicted as black or grey lines, with light grey areas indicating total variation (Max to Min) and dark grey areas representing quartiles (Q3 to Q1). Coloured lines, including temporal standard variation and pixel size (for reference), are read on the right vertical axis.

3.1.1. Stage 1

Fig. 7 presents the temporal statistics for each pixel along the SOI for Stage 1 using the FRACTAL algorithm with artificial lighting. In (*G1*) there is a significant variation in the detection of higher flows with R0-F15, R1-F15, R2-F15, and R3-F15 exhibiting the worst detection rates, as measurements consistently fall above the 1-pixel standard deviation. The minimum is often detected well below the observed values, resulting in unrealistic oscillations of up to 10 mm. This discrepancy was readily observable in the images, as the detection assumed the underside of the free surface (*i.e.*, the reflection of the bed on the surface – as shown in Fig. 6, (G1)) as the longest line in the ROI, and as such, the free

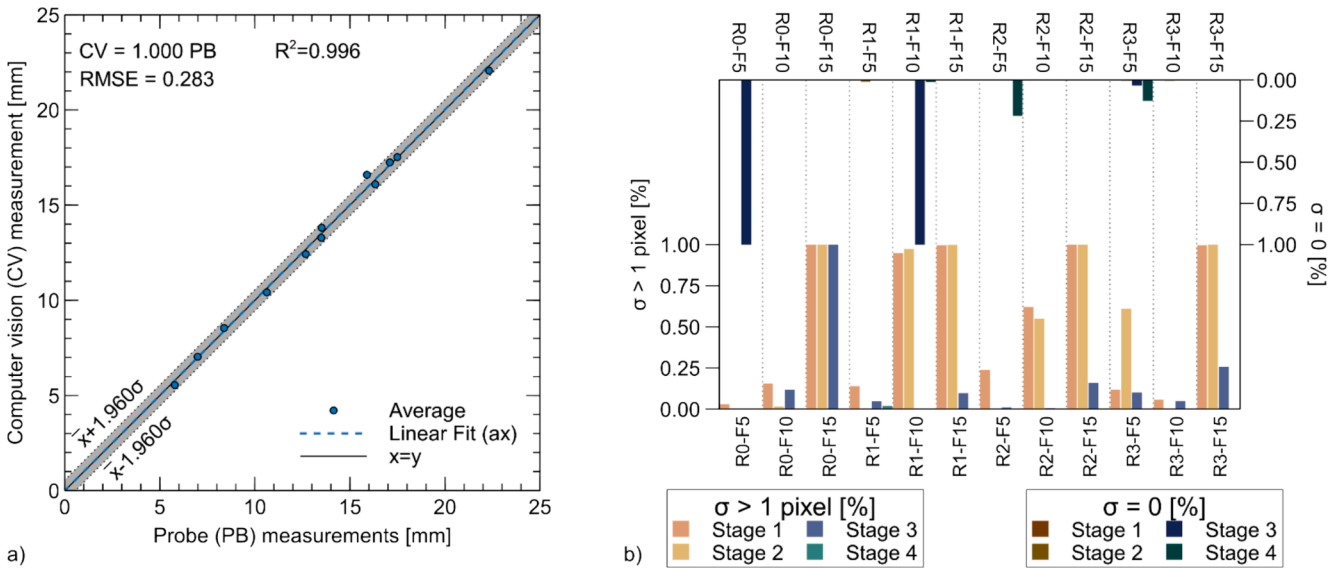

Fig. 12. A) graphical correlation between the averaged values obtained from the probes and the values generated by fractal, linear fitting, and fitting within the 95% confidence interval; b) summary of the total amount of deviation (s) for the different stages of the experiment, presented as the percentage of points that have a temporal variation higher than 1 pixel or equal to 0 (both indicate a low confidence in the correctness of the results).

Table 3
Summary of the dominant measurements group attributed to each test.

Stage	R0-F5	R0-F10	R0-F15	R1-F5	R1-F10	R1-F15	R2-F5	R2-F10	R2-F15	R3-F5	R3-F10	R3-F15
1	*G4*	*G2*	*G1*	*G1*	*G1*	*G1*	*G2*	*G1*	*G1*	*G2*	*G2*	*G1*
2	*G4*	*G1*	*G1*	*G4*	*G1*	*G1*	*G4*	*G1*	*G1*	*G3*	*G4*	*G1*
3	*G3*	*G4*	*G3*	*G4*	*G3*	*G4*	*G4*	*G4*	*G4*	*G4*	*G4*	*G4*
4	*G4*	*G4*	*G4*	*G4*	*G4*	*G4*	*G3*	*G4*	*G4*	*G3*	*G4*	*G4*

surface. It should be noted, however, that these erroneous detections were not common, but rather increased the variability of the measurement and introduced erroneous values. The high deviation between the mode and the average is also a signal of lack of accuracy. This effect is particularly visible in the abovementioned tests, and to a lesser extent in R1-F10 and R2-F10. R1-F5 shows residual erroneous values. Values of Q1 and Q3, on the other hand, remain within acceptable ranges, indicating that most detections are within 1 mm of the mode. In (*G2*) lower flows, namely R2-F5, R3-F5, R0-F10, and R3-F10 led to spurious detections occurring not in the reflection but in the top section of the ROI/SOI. This is visible in the sections between 400 and 500 pixels where the measured value is above 10 mm. (*G3*) points are nonexistant in this test stage. In (*G4*) R0-F5 shows a stable detection pattern, as evidenced by the below-pixel standard deviation and a maximum and minimum deviation below 1 mm, with only a few sections exhibiting deviations.

3.1.2. Stage 2

Fig. 8 illustrates the temporal statistics for each pixel along the SOI for Stage 2, using the FRACTAL algorithm with background subtraction, channel selecting, remapping, and artificial lighting. The enhancements translate into a higher correct detection rate when compared to Stage 1. In (*G1*), R0-F15, R1-F15, R2-F15, and R3-F15 still shows spurious detections on the underside reflection of the free surface on the far side of the channel (against the backwall), although variability remains within acceptable values despite the exaggerated detections. Averages are closer to the mode, with only three major areas with high variability: in R0-F15 from 0 to 450 pixels, in R1-F15 between 0 and 200 pixels, in R2-F15 between 300 and 400 pixels, and in R3-F15 between 400 and 500 pixels. R1-F10 and R2-F10 show a higher detection rate when compared to Stage 1 and a decrease in spurious detections. Moreover, Stage 2 tests present averages closer to the mode. In R0-F10 the underside of the free surface was detected in a small section between 0 and 100 pixels. (*G2*) is not present in the context of Stage 2. In (*G3*), R3-F5 presented worse results when compared to Stage 1, especially when considering variability, as the distance between quartiles becomes larger compared to other measurements. This inconsistency is attributed to the non-detection of part of the temporal range. The averaged measurements are also higher than in Stage 1. R1-F5 presents a section, between 550 and 600 pixels, where the non-detection is visible, with the standard deviation going below 10^{-2} mm. In (*G4*), R0-F5, R1-F5, R2-F5, R0-F10, and R3-F10 no longer show detection of the ceiling values detected in (Stage 1). It's worth noting that the same videos were used both in Stage 1 and Stage 2.

3.1.3. Stage 3

Fig. 9 presents the temporal statistics for each pixel along the SOI for Stage 3, using the FRACTAL algorithm, tinted water, and without background subtraction and artificial lighting. Although introducing water tinting and removing artificial lighting improved the overall results, some unforeseen issues were detected. In (*G1*) the detection of reflections on the underside of the free surface were eliminated. Applying tint to the water, thereby simulating natural conditions characterised by turbidity or the presence of coloured particles that render the water somewhat opaque, results in the elimination of the detection of underside reflections, thereby significantly enhancing accuracy. In (*G2*) the spurious detection of values above the free surface were also eliminated. The observed phenomenon can be ascribed to the use of enhancements 4 and 5, specifically the augmentation of contrast, which effectively eliminates detections on the white paper that constitutes the backwall of the channel. In (*G3*) the measurements' variability was acceptable in all the tests. However, the main issue, as seen in R0-F15, R0-F5, and R1-F10, was related to the non-detection of the free

Table 4
Differences (%), PBIAS (%), and RMSE between the average values derived from the probe's measurements and those obtained from FRACTAL.

	R0-5	R0-10	R0-15	R1-5	R1-10	R1-15	R2-5	R2-10	R2-15	R3-5	R3-10	R3-15
Differences	4.1	1.9	1.5	−0.6	1.5	−0.2	−2.0	−2.2	−0.9	2.0	−4.4	1.1
PBIAS	5.3	2.9	0.5	−2.3	1.9	0.3	−2.9	−2.2	−1.4	2.2	−4.0	0.9
RMSE	0.318	0.326	0.116	0.185	0.272	0.071	0.244	0.307	0.243	0.282	0.639	0.211

surface, either for the whole time, or for a section of time within the measuring frames (R0-F15). The observed phenomenon can be attributed to the reduced luminosity experienced during Stages 3 and 4, which contrasted with the higher luminosity observed during Stages 1 and 2, thereby affecting the accuracy of measurements and, therefore, the accuracy of measurements. Additionally, the absence of background removal further contributed to the failure in detecting the free surface due to the lower contrast between air and water. Nevertheless, the elimination of artificial lighting during testing was considered necessary, as the tests in laboratory are often conducted with different levels of lighting. In these tests, the variability (standard deviation) was mostly within 1 pixel. All the other tests, R0-F10, R1-F5, R1-F15 as well as all R2 and R3 tests, performed within (*G4*).

3.1.4. Stage 4

Fig. 10 illustrates the temporal statistical analysis conducted on each pixel along the section of interest (SOI) during Stage 4, using the FRACTAL algorithm. The experiments involved the use of tinted water, background subtraction and the absence of artificial lighting. Most of the results fall within the range denoted as (*G4*). Conversely, (*G1*) and (*G2*) are not observed due to the complete elimination of detection of the upper section and under-surface reflection, respectively. This resulted from the implementation of background subtraction and water tinting. However, there are some instances of non-detections, referred to as (*G3*), occurring at R2-F5 between 125 and 175 pixels as well as between 450 and 575 pixels. Non-detections are also observed at R3-F5, in localised regions with standard deviations below 10^{-2} and scattered throughout the section. Furthermore, a 10-pixel length section near 100 pixels in R1-F10 exhibits localised non-detections. Through all tests, the average variability remains below one pixel, with a minor exception observed between 550 and 600 pixels (in R1-F5). Notably, the observed variability falling between 10^{-2} mm and 1 pixel demonstrates an excellent agreement with the observed values.

3.2. Validation of FRACTAL improvements (Stage 4)

Fig. 11 a) depicts the comparison of data acquired from the ultrasonic sensor against the data generated by the FRACTAL algorithm. Direct comparison between these two datasets was hindered by certain limitations. The ultrasonic sensor failed to provide accurate measurements near the channel walls, whilst the FRACTAL algorithm cannot measure depths at the centre of the channel. To ensure that the hydraulic conditions remained consistent, the ultrasonic sensor was strategically placed, and measurements of FRACTAL were compared with the sensor's measurements in the direction projected against the walls. Measurements generally fell within a similar range to the computer vision technique, although the probe exhibited higher variability as seen in Fig. 11 b). This disparity can be attributed to two primary factors. Firstly, the location at which the sensor measured the depth differed from the CV technique. As the probe focused on the centre of the channel instead of the walls, variations in flow depth were more pronounced and unstable due to turbulence and the presence of reflective waves (from the walls and bed). Upon considering a moving average with 10 data points, the values converged to an average difference of less than 1 mm, with a maximum deviation of approximately 2 mm (see Fig. 12 a)). Secondly, the ultrasonic device measured the surface elevation within an approximately 1 cm2 region once per second, retaining the highest recorded value in the section. This measurement methodology, can be affected by rapidly changing free surface oscillations, leads to discrepancies when comparing measurements. Fig. 11 b) shows the boxplot for each of the tests and includes outliers for the probe values. It is noteworthy that nearly 5 % of probes measurements are considered outliers. This is clearly visible in Fig. 11 a), when outlier marks (points) are very far from the moving average, as some spurious values are clearly visible. Reasoning behind this phenomenon is related to the area the sensor measures and the oscillations of the free surface. No de-spiking technique was used, and data presented is raw. Other than the outlier, and although the probes do exhibit a more oscillatory behaviour, the averages, Q1 and Q3 are close, with differences of less than 5 % between them as seen in Table 4.

Fig. 12 a) presents the graphical representation of the correlation between the averaged values acquired with the ultrasonic sensor and the corresponding values obtained using the FRACTAL algorithm. On average, a strong correlation is observed ($R^2 = 0.996$), with most values falling within the 95 % confidence interval. However, due to the different measurement locations employed (the centre of the channel for the probe and the wall for the camera), a direct correlation without applying averaging was unattainable. Fig. 12 b) provides a comprehensive overview of the results obtained from the four stages considered. In Stage 1, a notable variability error was observed, indicating relatively high levels of uncertainty. Stage 2 demonstrated improvements compared to Stage 1, yet still exhibited somewhat high error levels. Stage 3 enhancements shown non-detections. Lastly, Stage 4 did not present erroneous measurements, despite some localised non-detections.

Overall Stage 4 outperformed all preceding stages, providing compelling evidence that the introduced improvements significantly enhance the FRACTAL computer vision algorithm. These improvements resulted in superior detection capabilities and a notable reduction in spurious results.

4. Discussion on the identified shortcomings of the methodology and possible extensibility to other applications

To address the identified shortcomings of our methodology and consider its potential for other uses, we analysed its limitations. Our goal is to transparently recognise areas needing improvement and explore alternative strategies to strengthen the methodology. Additionally, we assessed how adaptable the method is to various applications beyond our study's scope. By examining broader implications and potential extensions, we aimed to foster discussion on the method's versatility and applicability. We've summarised the shortcomings and potential extensions below:

- In laboratory settings, surface tension may affect measurements under specific conditions. This effect becomes more noticeable when precision requirements are high and flow depth is shallow. Increased precision (e.g., closer camera proximity) and shallower flow depths can significantly impact measurements due to surface tension. However, in field settings where cameras are positioned farther away and flow depths are greater, the influence of surface tension is expected to be minimal.
- Blurred and low-quality images may pose a challenge due to reduced clarity. However, this limitation affects more precision rather than accuracy if the measurer is aware of it. Artificial lighting can mitigate this issue.

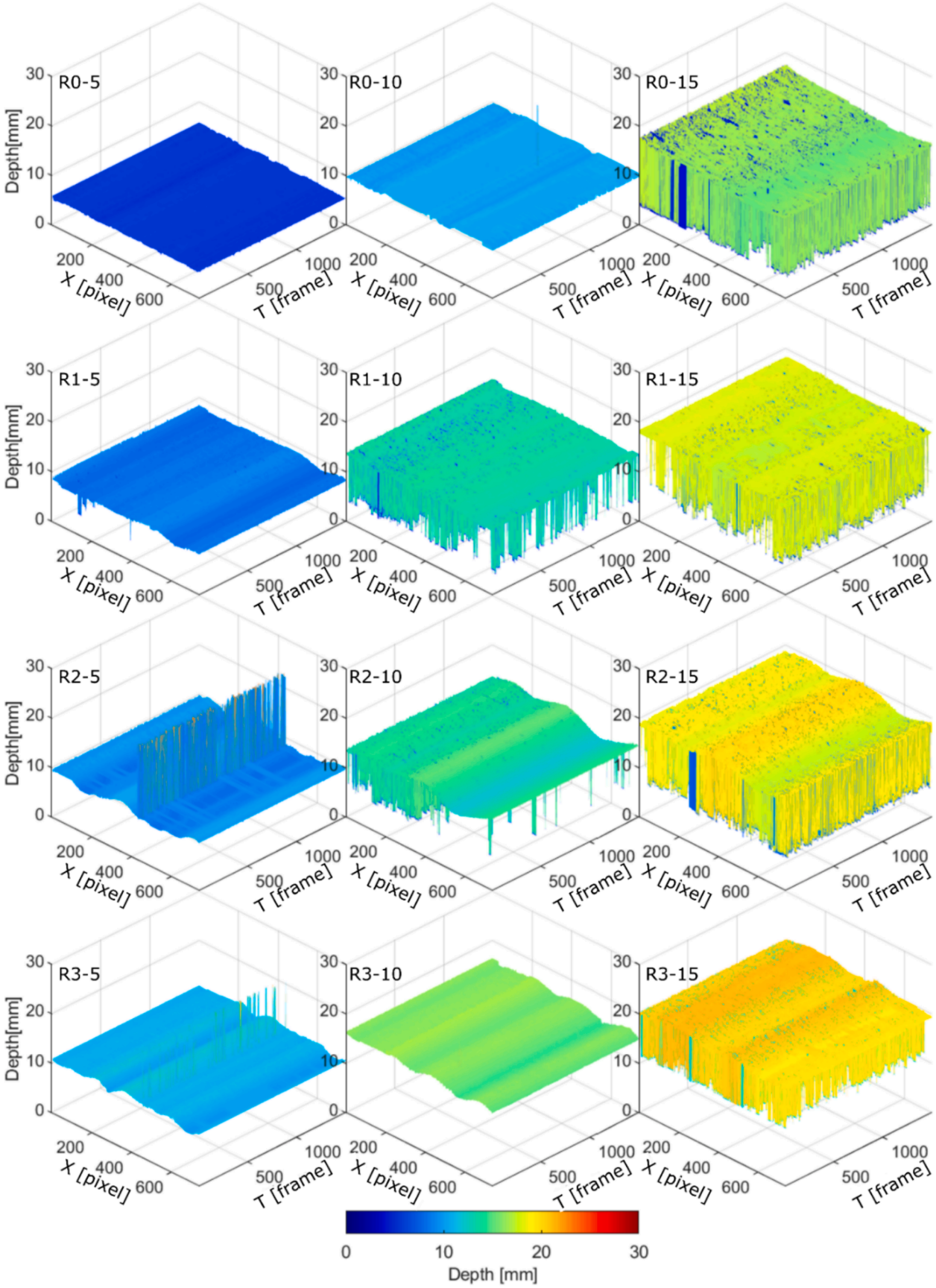

Fig. 13. 3D plot of the measured surface in time and space for the SOI using the FRACTAL algorithm (Stage 1).

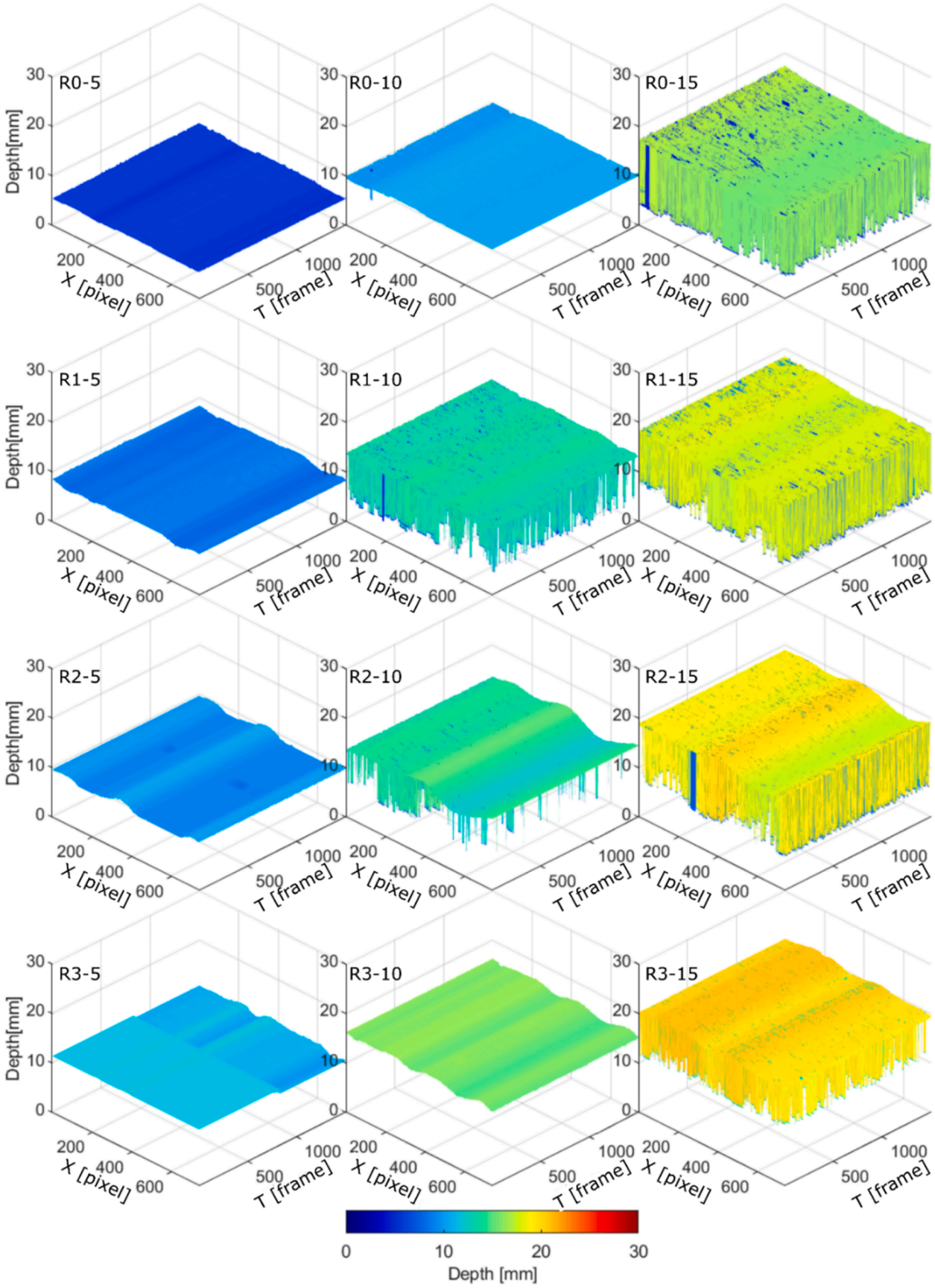

Fig. 14. 3D plot of the measured surface in time and space for the SOI using the FRACTAL algorithm (Stage 2).

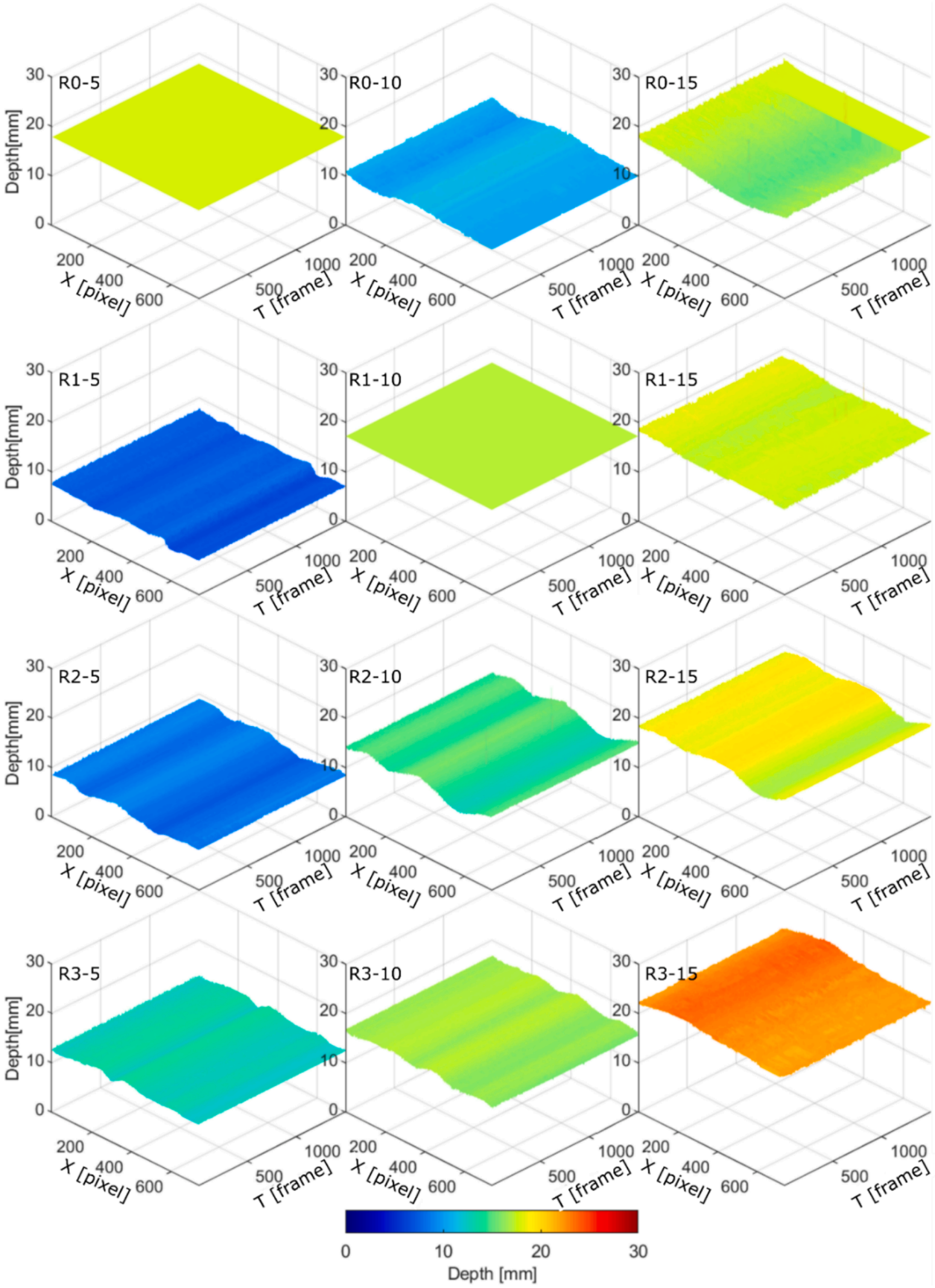

Fig. 15. 3D plot of the measured surface in time and space for the SOI using the FRACTAL algorithm (Stage 3).

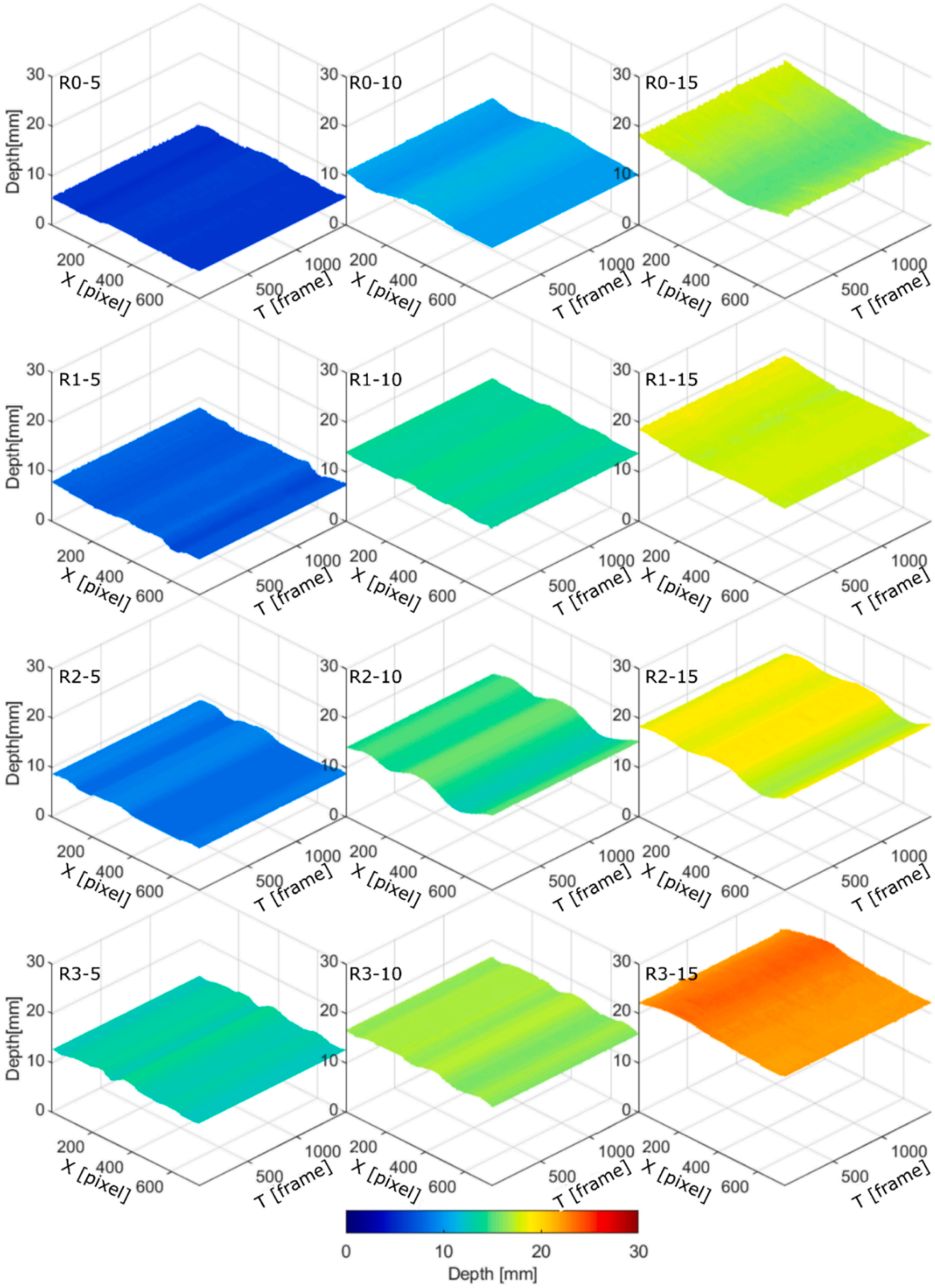

Fig. 16. 3D plot of the measured surface in time and space for the SOI using the FRACTAL algorithm (Stage 4).

- This measurement method is suitable for 1D flows but may not fully capture features in 2D or 3D flows. Nevertheless, it offers an improvement over conventional techniques like pressure or depth sensors as it allows for lengthwise measurements.
- The methodology shows promise for extension to river/sea depths by contrasting the surface images against piers, walls, bridges, and channels.

5. Conclusions

This study presents a computer vision based technique that significantly enhances the detection and measurement of high-frequency fluctuations in the free surface through transparent walls in laboratory channels. A key-enhancement of this methodology comes from subtracting the background from the imagery under processing. The results suggest that tinting the water and adding artificial lighting can improve the accuracy of the measurements. However, these approaches may not universally yield better measurement results. To ensure the accuracy and reliability of the results obtained through the computer vision based technique, rigorous validation was performed by comparing them against measurements recorded using state-of-the-art high-resolution ultrasonic sensors.

The Stage 4 FRACTAL algorithm demonstrates superior performance compared to all test iterations (Stages 1, 2, and 3) and conventional methods, such as ultrasonic sensors. Specifically, it enables spatial (longitudinal) and temporal measurement of the free surface, while being non-intrusive (*i.e.*, not disturbing the flow field), but at the same time cost-effective, whilst other techniques do not allow for such a high spatial and temporal resolution.

The results also exhibited excellent agreement and strong correlation ($R^2 = 0.996$) with well-established methods, thus validating the proposed technique, including the five enhancements implemented in the FRACTAL algorithm, *i.e.*, background subtraction (1), channel selecting (2), remapping and increasing contrast (3), and the tinting of water (4) as well as gradient weighting (5) for increased contrast. More specifically:

(1) The employed background removal technique effectively improves the air–water interface detection by emphasising the dynamic component, representing the changing elements in the image.
(2) Channel selection enhances contrast by capitalising on the absence of blue in the water and on the prevalence of blue in the wall white background.
(3) Remapping techniques eliminate extreme values of luminosity and the blue channel, leading to a more accurate depiction of the air–water interface.
(4) Tinting the water aids in eliminating the detection of high-luminosity beneath the surface reflections. The contrast enhancement process refines local contrast by smoothing areas with low gradients while preserving strong edges.
(5) Additionally, the application of gradient weighting enables a balanced consideration of information from both sources, resulting in a cleaner final output image that enhances accuracy in processing the air–water interface.

CRediT authorship contribution statement

Ricardo Martins: Writing – review & editing, Writing – original draft, Visualization, Validation, Software, Methodology, Investigation, Formal analysis, Conceptualization, Data curation. **Jorge M.G.P. Isidoro:** Writing – review & editing, Writing – original draft, Validation, Methodology, Formal analysis, Conceptualization. **João L.M.P. de Lima:** Writing – review & editing, Supervision, Funding acquisition.

Declaration of competing interest

The authors declare that they have no known competing financial interests or personal relationships that could have appeared to influence the work reported in this paper.

Data availability

Videos used in this paper are available at https://dx.doi.org/10.5281/zenodo.13341390 under CC BY-NC-ND 4.0.

Acknowledgements

Ricardo Martins was supported by the FCT through the Research Centre for Risks and Sustainability in Construction (RISCO), University of Aveiro, Portugal [grant number UIDP/04450/2020 + UIDB/04450/2020]. This study also had the support of Portuguese funds through *Science and Technology Foundation* (FCT), under the projects [grant numbers UIDB/04292/2020, UIDP/04292/2020] granted to MARE, Marine and Environmental Sciences Centre, [grant UIDB/00350/2020] granted to CIMA, Centre for Marine and Environmental Research, and [grant number LA/P/0069/2020] granted to the *Associate Laboratory ARNET*, Aquatic Research Network. The tests and manuscript were started with Jorge Isidoro as a member of MARE and concluded as a member of CIMA. The tests were conducted at the Laboratory of Hydraulics, Water Resources and Environment, at the Department of Civil Engineering of the University of Coimbra, in Portugal. Videos used in this paper can be downloaded at https://dx.doi.org/10.5281/zenodo.13341390.

Appendix A

References

Bertrand-Krajewski, J.L., Laplace, D., Joannis, C., Chebbo, G., 2008. Mesures en hydrologie urbaine et assainissement, Tec & Doc. ed.
Chaudhary, P., D'Aronco, S., Leitão, J.P., Schindler, K., Wegner, J.D., 2020. Water level prediction from social media images with a multi-task ranking approach. ISPRS J. Photogramm. Remote Sens. 167, 252–262. https://doi.org/10.1016/j.isprsjprs.2020.07.003.
Fernandes, F.E., Nonato, L.G., Ueyama, J., 2022. A river flooding detection system based on deep learning and computer vision. Multimed. Tools Appl. 81, 40231–40251. https://doi.org/10.1007/s11042-022-12813-3.
Forsyth, D.A., Ponce, J., 2002. Computer vision: a modern approach. Prentice hall professional technical reference.
Gilmore, T.E., Birgand, F., Chapman, K.W., 2013. Source and magnitude of error in an inexpensive image-based water level measurement system. J. Hydrol. (Amst.) 496, 178–186. https://doi.org/10.1016/j.jhydrol.2013.05.011.
Gupta, V.K., Mittal, A., Gajbe, V., 2005. Adsorption and desorption studies of a water soluble dye, Quinoline Yellow, using waste materials. J. Colloid Interface Sci. 284, 89–98. https://doi.org/10.1016/j.jcis.2004.09.055.
Herschy, R.W., 2008. Streamflow Measurement. CRC Press.
Huang, K., Chen, H., Xiang, T., Lin, Y., Liu, B., Wang, J., Liu, D., Xu, C.-Y., 2022. A photogrammetry-based variational optimization method for river surface velocity measurement. J. Hydrol. (Amst.) 605, 127240. https://doi.org/10.1016/j.jhydrol.2021.127240.
Isidoro, J.M.G.P., Martins, R., Carvalho, R.F., de Lima, J.L.M.P., 2021. A high-frequency low-cost technique for measuring small-scale water level fluctuations using computer vision. Measurement 180, 109477. https://doi.org/10.1016/j.measurement.2021.109477.
Isidoro, J.M.G.P., Martins, R., Pereira, L.G., de Lima, J.L.M.P., 2023. Design and characterisation of customised-roughness beds for open-channel flow experiments. Flow Meas. Instrum. 94, 102472. https://doi.org/10.1016/j.flowmeasinst.2023.102472.
Jafari, N.H., Li, X., Chen, Q., Le, C.-Y., Betzer, L.P., Liang, Y., 2021. Real-time water level monitoring using live cameras and computer vision techniques. Comput. Geosci. 147, 104642. https://doi.org/10.1016/j.cageo.2020.104642.
Jawad, H.M., Husain, T.A., 2017. Measuring object dimensions and its distances based on image processing technique by analysis the image using Sony camera. Euras. J. Sci. Eng. 3. https://doi.org/10.23918/eajse.v3i2p100.
Ji, H., Yoo, S., Lee, B.-J., Koo, D., Kang, J.-H., 2020. Measurement of wastewater discharge in sewer pipes using image analysis. Water (Basel) 12, 1771. https://doi.org/10.3390/w12061771.

Kuswidiyanto, L.W., Nugroho, A.P., Jati, A.W., Wismoyo, G.W., Murtiningrum, Arif, S.A., 2021. Automatic water level monitoring system based on computer vision technology for supporting the irrigation modernization. IOP Conf. Ser. Earth Environ. Sci. 686, 012055. https://doi.org/10.1088/1755-1315/686/1/012055.

Lan, Y., Han, D., Bai, F., Zhong, Z., Weng, Z., 2020. Review of Research and Application of Fluid Flow Detection Based on Computer Vision, in: Proceedings of the 4th International Conference on Computer Science and Application Engineering. ACM, New York, NY, USA, pp. 1–8. https://doi.org/10.1145/3424978.3425112.

Leo, M., Natale, A., Del-Coco, M., Carcagnì, P., Distante, C., 2017. Robust estimation of object dimensions and external defect detection with a low-cost sensor. J. Nondestr. Eval. 36, 17. https://doi.org/10.1007/s10921-017-0395-7.

Lin, Y.-T., Lin, Y.-C., Han, J.-Y., 2018. Automatic water-level detection using single-camera images with varied poses. Measurement 127, 167–174. https://doi.org/10.1016/j.measurement.2018.05.100.

Loizou, K., Koutroulis, E., 2016. Water level sensing: State of the art review and performance evaluation of a low-cost measurement system. Measurement 89, 204–214. https://doi.org/10.1016/j.measurement.2016.04.019.

Majdalani, S., Chazarin, J.-P., Moussa, R., 2019. A new water level measurement method combining infrared sensors and floats for applications on laboratory scale channel under unsteady flow regime. Sensors 19, 1511. https://doi.org/10.3390/s19071511.

Moozyckine, A.U., Davies, D.M., 2002. Green S as a prototype for an environmentally-degradable dye: the concept of a 'green dye' in future Green Chemistry. Green Chem. 4, 452–458. https://doi.org/10.1039/B204556G.

Nguyen, L.S., Schaeli, B., Sage, D., Kayal, S., Jeanbourquin, D., Barry, D.A., Rossi, L., 2009. Vision-based system for the control and measurement of wastewater flow rate in sewer systems. Water Sci. Technol. 60, 2281–2289. https://doi.org/10.2166/wst.2009.659.

Noto, S., Tauro, F., Petroselli, A., Apollonio, C., Botter, G., Grimaldi, S., 2022. Low-cost stage-camera system for continuous water-level monitoring in ephemeral streams. Hydrol. Sci. J. 67, 1439–1448. https://doi.org/10.1080/02626667.2022.2079415.

Sabbatini, L., Palma, L., Belli, A., Sini, F., Pierleoni, P., 2021. A computer vision system for staff gauge in river flood monitoring. Inventions 6, 79. https://doi.org/10.3390/inventions6040079.

Sinha, P.K., 2012. Image acquisition and preprocessing for machine vision systems. SPIE. Doi 10 (1117/3), 858360.

Sobel, I., Feldman, G., 1968, "A 3x3 Isotropic Gradient Operator for Image Processing", presented in a talk at the Stanford Artificial Intelligence Project (SAIL) in 1968.

Zhang, D., Tong, J., 2023. Robust water level measurement method based on computer vision. J. Hydrol. (Amst.) 620. https://doi.org/10.1016/j.jhydrol.2023.129456.